Inorganic Chemistry
Article

Inorg. Chem. **2010**, *49*, 10687–10693 **10687**
DOI: 10.1021/ic1015127

Isomorphous Substitutions of Rare Earth Elements for Calcium in Synthetic Hydroxyapatites

Lyudmyla I. Ardanova,*,† Evgeni I. Get'man,‡ Stanislav N. Loboda,‡ Vadim V. Prisedsky,§ Tatiana V. Tkachenko,‡ Valeriy I. Marchenko,‡ Valeriy P. Antonovich,∥ Nataliya A. Chivireva,∥ Konstantin A. Chebishev,‡ and Alexandra S. Lyashenko‡

†*Department of Chemistry and Geology, Minnesota State University, Mankato, 241 Ford Hall, Mankato, Minnesota 56001 United States* , ‡*Department of Inorganic Chemistry, Donetsk National University, 24 Universitetskaya, Donetsk 83001, Ukraine,* §*Department of General Chemistry, Donetsk National Technical University, 58 Artema, Donetsk 83001, Ukraine, and* ∥*A.V. Bogatsky Physico-Chemical Institute, National Academy of Sciences, 86 Lustdorfskaya doroga, Odessa 65080, Ukraine*

Received August 23, 2010

Polycrystalline hydroxyapatites $Ca_{10-x}REE_x(PO_4)_6(OH)_{2-x}O_x$ were synthesized and studied by X-ray powder diffraction, infrared absorption, diffuse-reflectance spectroscopy, and thermogravimetry. The solubility limits x_{max} of rare earth elements (REE) in Ca hydroxyapatites decreases with an increasing REE atomic number from $x_{max} = 2.00$ for La, Pr, and Nd to $x_{max} = 0.20$ for Yb at 1100 °C. Refinements of X-ray diffraction patterns by the Rietveld method show that REE atoms substitute for Ca preferentially at the Ca(2) sites of the apatite structure. The substitution decreases the Ca(2)−O(4) atomic distances in the calcium coordination polyhedra and increases the Ca(2)−O(1,2,3) distances. This observation shows that interatomic distances depend not only on radii of the ions involved in the substitution but also on their charges.

1. Introduction

Compounds with the apatite structure have the general composition $M_{10}(EO_4)_6(X)_2$, where M is a univalent to trivalent cation (Ca^{2+}, Sr^{2+}, Ba^{2+}, Cd^{2+}, Eu^{3+}, Y^{3+}, La^{3+}, Na^{1+}, K^{+1}, etc), E is a tetravalent to hexavalent element (P^{5+}, V^{5+}, As^{5+}, Si^{4+}, Ge^{4+}, S^{6+}, Cr^{6+}, etc.), and X represents anions OH^-, F^-, Cl^-, Br^-, I^-, and O^{2-}. Calcium hydroxyapatite $Ca_{10}(PO_4)_6(OH)_2$ is particularly interesting among them because of its chemical similarity to the principal inorganic constituent of bone tissue. Due to its absolute biocompatibility with living tissues, calcium hydroxyapatite ceramics are widely used as biomaterials in medicine (stomatology, maxillofacial surgery, orthopedics, and traumatology).[1−5] In addition, hydroxyapatites can be used as adsorbents of toxic components from both liquid (adsorbing ions of Cl, F, Pb, Cu, Cd, U, Pu, As, Se, etc.) and gas (adsorbing aliphatic and aromatic hydrocarbons, ammonia, carbon oxides, pathogenic microbes, viruses, etc.) phases.[6−20] They are also used as adsorbents in chromatography, including separation of proteins and nucleic acids, and also have application in the purification of human proteins.[21] Calcium hydroxyapatite and its

*Corresponding author. E-mail: lyudmyla.ardanova@mnsu.edu. Telephone: 507-389-1999.

(1) Kanazawa, T. *Inorganic Phosphate Materials*; Elsevier: Amsterdam, The Netherlands, 1989.
(2) Suchanek, W.; Yoshimura, M. *J. Mater. Res.* **1998**, *13*, 94–117.
(3) Gross, K. A.; Berndt, C. C. *Rev. Mineral. Geochem.* **2002**, *48*, 631–672.
(4) Douglas, T.; Pamula, E.; Hauk, D.; Wiltfang, J.; Sivananthan, S.; Sherry, E.; Warnke, P. *Mater. Med.* **2009**, *20*(9), 1909–1915.
(5) Zhang, J.; Iwasa, M.; Kotobuki, N.; Tanaka, T.; Hirose, M.; Ohgushi, H.; Jiang, D. *J. Am. Ceram. Soc.* **2006**, *89*, 3348–3355.
(6) Smiciklas, I.; Milonjic, S.; Pfendt, P.; Raicevic, S. *Sep. Purif. Technol.* **2000**, *18*, 185–194.
(7) Monteil-Rivera, F.; Fedoroff, M.; Jeanjean, J.; Minel, L.; Barthes, M.-G.; Dumonceau, J. *J. Colloid Interface Sci.* **2000**, *221*, 291–300.
(8) Jeanjean, J.; McGrellis, S.; Rouchaud, J. C.; Fedoroff, M.; Rondeau, A.; Perocheau, S.; Dubis, A. *J. Solid State Chem.* **1996**, *126*, 195–201.
(9) Sugiyama, S.; Matsumoto, H; Hayashi, H.; Moffat, J. *Colloids Surf., A* **2000**, *169*, 17–26.
(10) Fuller, C.; Bargar, J; Davis, J.; Piana, M. *Environ. Sci. Technol.* **2002**, *36*, 158–165.
(11) Mavropoulos, E.; Rossi, A.; Costa, A.; Perez, C.; Moreira, J; Saldanha, M. *Environ. Sci. Technol.* **2002**, *36*, 1625–1629.
(12) Akihiko, Y.; Tetsuro, O. Deodorants, deodorant sheets, filter sheets and functional papers as well as filtering mediums for exhaust gas. U.S. Patent, 5567231, 1996.
(13) Leyva, A.; Marrero, J; Smichowski, P.; Cicerone, D. *Environ. Sci. Technol.* **2001**, *35*, 3669–3675.
(14) Cheung, C.; Porter, J.; McKay, G. *Langmuir* **2002**, *18*, 650–656.
(15) Kandori, K.; Mukai, M.; Fujiwara, A.; Yasukawa, A.; Ishikawa, T. *J. Colloid Interface Sci.* **1999**, *212*, 600–603.
(16) Kandori, K.; Mukai, M.; Yasukawa, A.; Ishikawa, T. *Langmuir* **2000**, *16*, 2301–2305.
(17) Luo, Q.; Andrade, J. *J. Colloid Interface Sci.* **1998**, *200*, 104–113.
(18) Kandori, K.; Horigami, N.; Kobayashi, H.; Yasukawa, A.; Ishikawa, T. *J. Colloid Interface Sci.* **1997**, 498–502.
(19) Barroug, A.; Lernoux, E.; Lemaitre, J.; Rouxhet, P. *J. Colloid Interface Sci.* **1998**, *208*, 147–152.
(20) Thakur, P.; Moore, R.; Choppin, G. *Radiochim. Acta* **2006**, *94*, 9–11.
(21) Shepard, S.; Schrimsher, J.; Schrimsher, J. *J. Chromatogr., A* **2000**, *891*, 93–98.

Published on Web 10/19/2010

derivatives are also used in gas sensors,[22,23] luminescent[24,25] and laser materials,[27,28] mercury tubes,[29] catalysts in organic reactions involving conversion of methane, dehydration of alcohol, hydrolysis of chlorobenzene, and others.[30−43] They can also be effectively used for nuclear waste disposal.[44]

Hydroxyapatites modified by substitution of their constituents for atoms of other elements have better catalytic (Pb, Cu),[30−34] sensor (Na),[22] and antimicrobial properties (Ag)[35] than does pure hydroxyapatite. Hydroxyapatites with complete substitution of vanadium for phosphorus have enhanced catalytic properties[42] and have been used as carriers for palladium, ruthenium complexes, zinc, nickel, and copper compounds[37,39,40] in heterogeneous hybrid catalysis.

As is typically the case, chemical and physical properties change in a regular fashion with the degree of substitution within the hydroxyapatite solid solution region. Thus, information about the compositional limit of a particular dopant in the apatite structure is crucial for formulating a synthetic apatite having the desired properties. In some instances, a very low concentration of dopant can result in desired properties. For example, in luminescent and laser materials the concentration of dopant is about 1% and lower,[27] while in a strontium hydroxyapatite catalyst modified by lead, the concentration of Pb is 33%.[43]

Substitutions also change interatomic distances in the structure and thereby affect adsorptive, catalytic, and sensor properties. According to Balandin's geometrical theory of catalysis, atomic arrangements on the contact surfaces in a case of chemosorption have to be in agreement with the geometry of adsorbed molecules of reactants.[45] Adsorption of organic molecules by hydroxyapatite is caused by hydrogen-bond formation between these molecules and O^{2-} or OH^- anions of hydroxyapatite.[1] For example, increased catalytic activity of modified strontium hydroxyapatite is due to a change in the Sr−O interatomic distance as a result of partial substitution of Pb for Sr in the apatite structure.[26,46]

Ca, Sr, and Ba hydroxyapatites are often modified by Pb. In isovalent substitutions, interatomic distances typically change monotonically with change in composition, which makes it possible to calculate these distances in the structure of solid solutions. For example, substitution of larger Ba^{2+} for smaller Sr^{2+} in the structure of $Sr_{10}(VO_4)_6(OH)_2$ increases the distances Sr(1)−O(1,2,3), Sr(2)−O(1,2,3), Sr(2)−Sr(2), and Sr(2)−OH.[47]

Hydroxyapatites modified by trivalent elements are used less, and there is only limited information on this type of isomorphous substitution and resultant modification of interatomic distances. The substitution of trivalent lanthanum and rare earth elements for calcium in phosphate hydroxyapatite has been studied in ref , taking into account the similarity of their radii (r) to that of Ca^{2+} in the apatite structure (1.300 (La^{3+})−1.117 Å (Lu^{3+}) as compared to 1.26 Å (Ca^{2+}) for CN = 8).[48] As a result of substitution under the scheme: $Ca^{2+} + OH^- \rightarrow La^{3+} + O^{2-}$, mean distances Ca(2)−O(1,2,3) increase by approximately 0.13 Å due to location of larger La^{3+} cations in Ca(2)−O polyhedra, but some interatomic distances decrease, for example, Ca(2)−OH(O4) from 2.380 to 2.143 Å, Ca(2)−Ca(2) from 4.052 to 3.711 Å, and P−O from 1.563 to 1.541 Å.[49] Authors concluded that these decreases in interatomic spacing resulted from increasing electrostatic interaction caused by substitution of highly charged ions (La^{3+}, O^{2-}) for less-charged ions (Ca^{2+}, OH^-) and that properties are affected to a greater extent by charges of the ions involved in the substitution than by their radii.

To evaluate controls on the mean interatomic distances in other systems, investigation of isomorphic replacements with a suite of rare earth elements is required. Isomorphic substitutions of Nd^{3+} and Dy^{3+} for Ca^{2+} (r = 1.25, 1.17, and 1.26 Å, respectively) were studied earlier.[50] Introduction of these two ions into the hydroxyapatite structure would be expected to result in a decrease of Ca(2)−O(1,2,3) distances, since Nd^{3+} radius is smaller than Ca^{2+} (by 0.01 Å), and Dy^{3+} radius is significantly smaller than Ca^{2+} (by 0.09 Å), but instead the Ca(2) − O(1,2,3) distances increase by 0.08 and 0.05 Å, respectively.[50] These examples indicate that prediction of particular interatomic distances in substituted apatites, hence catalytic activity of their solid solutions, requires further study.

To evaluate systematic changes in mean interatomic distances in the structure of Ca-phosphate hydroxyapatite as a result of heterovalent substitution of rare earth elements for calcium, we conducted further investigation with selected rare earth elements, specifically Pr, Sm, Gd, Tb, Ho, Er, Tm,

(22) Komine, Y.; Sato, K. *Fine Ceramics FC. Rep. 1* **1983**, 4–10.
(23) Tadashi, N.; Masayuki, N. Method of detecting carbon dioxide gas. U.S. Patent 4755473, 1998.
(24) Boyer, L.; Piriou, B.; Carpena, J.; Lacout, J. *J. Alloys Compd.* **2000**, *311*, 143–152.
(25) Goutaudier, C.; Dujardin, C.; Boulon, G.; Kbir-Ariguib, N.; Trabelsi-Ayedi, M. *Solid State Sci.* **2002**, *4*, 53–59.
(26) Zhu, K; Yanagisawa, K.; Shimanouchi, R.; Onda, A.; Kajiyoshi, K.; Qio, J. *Journal of the Ceramic Society of Japan* **2007**, *115*, 873–876.
(27) Payne, S. A.; Kway, W. L.; Deloach, L. D.; Krupke, W. F.; Chai, B. H. T. Ytterbium- and neodymium-doped vanadate laser hose crystals having the apatite crystal structure. U.S. Patent 5341389, 1994.
(28) Deutsch, N.; Schroder, T.; Stamm, U.; Zschocke, W. Q-switched solid-state laser. U.S. Patent 5838701, 1998.
(29) Thornton, W. A., Jr.; Unglert, M. C. Color-corrected high-pressure mercury-vapor lamp. U.S. Patent 3670194, 1972.
(30) Sugiyama, S.; Mitsuoka, H.; Shono, T.; Moriga, T.; Hayashi, H. *J. Chem. Eng. Jpn.* **2003**, *36*, 210–215.
(31) Matsumura, Y.; Sugiyama, S.; Hayashi, H.; Moffat, J *J. Solid State Chem.* **1995**, *114*, 138–145.
(32) Matsumura, Y.; Moffat, J.; Sagiyama, S.; Hayashi, H.; Shigemoto, N.; Saitoh, K. *J. Chem. Soc. Faraday Trans.* **1994**, *90*(14), 2133–2140.
(33) Sugiyama, S.; Moffat, J. B. *Catal. Lett.* **2002**, *81*, 77–81.
(34) Sugiyama, S.; Abe, K.; Hayashi, H.; Moffat, J. *Catal. Lett.* **1999**, *57*, 161–165.
(35) Edwards, N.; Mitchell, S. B.; Pratt, A. S. Silver compound antimicrobial compositions. U.S. Patent 3670194, 1972.
(36) Sugiyama, S.; Iguchi, Y.; Minami, T.; Hayashi, H.; Moffat, J. B. *Catal. Lett.* **1997**, *46*, 279–285.
(37) Yamaguchi, K; Mori, K.; Mizugaki, T.; Ebitani, K.; Kaneda, K. *J. Am. Chem. Soc.* **2000**, *122*, 7144–7145.
(38) Koutsopoulos, S.; Dalas, E. *Langmuir* **2000**, *16*, 6739–6744.
(39) Mori, K.; Yamaguchi, K.; Hara, T.; Mizugaki, T.; Ebitani, K.; Kaneda, K. *J. Am. Chem. Soc.* **2002**, *124*, 11572–11573.
(40) Sebti, S.; Tahir, R.; Nazih, R.; Boulaajaj, S. *Appl. Catal., A* **2001**, *218A*, 25–30.
(41) Sebti, S.; Tahir, R.; Nazih, R.; Saber, A.; Boulaajaj, S. *Appl. Catal., A* **2002**, *228A*, 155−159.
(42) Hara, T.; Kanai, S.; Mori, K.; Mizugaki, T.; Ebitani, K.; Jitsukawa, K; Kaneda, K. *J. Org. Chem.* **2006**, *71*, 7455–7462.
(43) Sugiyama, S.; Iguchi, Y.; Nishioka, H.; Miyamoto, T.; Hayashia, H.; Moffatb, J. *J. Mater. Chem.* **1997**, *7*(12), 2483–2487.
(44) Ewing, R. C. *Prog. Nucl. Energy* **2007**, *49*, 635–643.
(45) Balandin, A. A. *Adv. Catal.* **1958**, *10*, 96–129.
(46) Sugiyama, S.; Iguchi, Y.; Nishioka, H.; Minami, T.; Moriga, T.; Hayashi, H.; Moffat, J. B. *J. Catal.* **1998**, *176*, 25–34.
(47) Yablochkova, N; Get'man, E.; Marchenko, V.; Loboda, S. *Russ. J. Inorg. Chem.* **2008**, *53*, 850–853.
(48) Shannon, R. D. *Acta Crystallogr.* **1976**, *32A*, 751–767.
(49) Serret, A.; Cabanas, M. V.; Vallet-Regí, M. *Chem. Mater.* **2000**, *12*, 3836–3841.
(50) E.. Get'man, Loboda, S.; Tkachenko, T.; Ignatov, A.; Zabirko, T. *Funct. Mater.* **2005**, *12*, 6−10.

and Yb. Because vanadate apatites ($Ca_{10}(VO_4)_6(OH)_2$) also have high catalytic activity and yet have not been well-studied, we also report the limits of isomorphous substitutions of Ca in vanadate apatite for La, Nd, Sm, Eu, Gd, and Y.

2. Experimental Procedure

As starting reagents for apatite synthesis, we used $CaCO_3$, $(NH_4)_2HPO_4$ for phosphate apatites, NH_4VO_3 for vanadate apatites, and rare earth oxides REE_2O_3 (REE = La, Nd, Sm, Eu, Gd, Dy, Ho, Er, Tm, and Yb), Pr_6O_{11}, and Tb_4O_7. All reagents are provided by Sinbias (Ukraine) or Fisher Scientific (U.S.A.) and claimed by the manufactures to be 99.9% pure. In synthesizing hydroxyapatites we focused on attaining equilibrium in the studied systems at minimum temperatures, since hydroxyapatite decomposed to oxyapatite at temperatures of 1200 to 1400 °C.[49] The samples were prepared by three different methods.

Hydroxyapatites of composition $Ca_{10-x}REE_x(PO_4)_6(OH)_{2-x}O_x$, in which REE = Pr, Nd, Sm, and Dy, were synthesized by ceramic technology. One sample was prepared for each value of x in the preceding formula from 0 to 2.0 with an x increment of 0.2. A mixture of initial components with a total weight of 1.5 g was ground in a mortar, followed by successive annealing steps in alumina crucibles at 300 °C for 4 h, at 800 °C for 6 h, and finally at 1100 °C for about 30 h with intermittent grindings at the last temperature step. The duration of annealing for the last temperature step was determined by attaining stable phase composition of synthesized samples.

Attaining equilibrium and stable phase composition in $Ca_{10-x}REE_x(PO_4)_6(OH)_{2-x}O_x$ apatites becomes more difficult as REE atomic number increases. The systems in which REE = Pr and Sm take about 36 h and several intermittent grindings to reach equilibrium at 1100 °C. However, under the same conditions in the systems with REE = Gd, Tb, Ho, Er, Tm, and Yb, X-ray diffraction (XRD) analysis indicates that single phase samples cannot be formed, and the apatite phase is accompanied by β-$Ca_3(PO_4)_2$ (whitlockite) and a rare earth oxide phase. Increasing annealing duration to 54 h or raising the annealing temperature to 1200 °C does not result in a noticeable change in phase composition. These observations are indicative of a kinetically blocked reaction resulting in a state of pseudoequilibrium in the heavier REE system.

To overcome this difficulty, these samples were dissolved in 20−25 mL boiling water into which concentrated nitric acid (5−10 mL) was gradually added. The dry powder mixtures obtained after evaporation of such solutions were again annealed at 1100 °C for 48 h, resulting in homogeneous single-phase or heterogeneous multiphase samples with stable phase composition that did not change with longer times of annealing.

A third method was utilized for preparing vanadate apatite $Ca_{10-x}REE_x(VO_4)_6(OH)_{2-x}O_x$ samples. These samples were prepared by evaporation of the tartric acid solutions of above-listed components at 100 °C. The resulting dry residue was powdered and annealed for 6 h at 600 °C in a muffle oven. After grinding, samples were annealed for 20−80 h at 800 °C in a muffle oven with two intermittent grindings.

Phase composition of synthesized samples was determined by X-ray powder diffraction analysis. X-ray diffraction data were collected using DRON-2 and, for some samples, PANanalytical X'Pert PRO (PW 3040 PRO) diffractometers using Ni-filtered Cu K_α radiation at scanning rates 2°(2θ)/min (DRON-2) and 0.17°(2θ)/sec (PANanalytical X'Pert PRO). To improve the accuracy of measured interplanar distances, samples were rescanned at 0.25°(2θ)/min (DRON-2) and 0.03°(2θ)/sec (PANanalytical X'Pert PRO). Cerium dioxide or silicon were added to samples as an internal standard. To obtain data for crystal structure refinement, the samples were scanned in steps of 0.05° 2θ in the range 15° ≤ 2θ ≤ 140°, using a counting time of 10 s/step. The data were analyzed using the Rietveld procedure with the program FullProf.2k (version 4.50)[51] and the WinPLOTR software.[52]

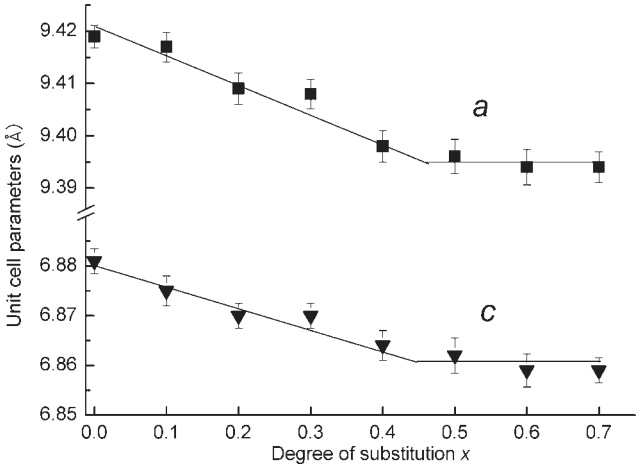

Figure 1. Plot of hexagonal unit cell parameters a and c vs degree of Tm substitution for calcium in phosphate hydroxyapatite.

To investigate the effect of substitutions on the apatites' hydroxyl content, infrared absorption spectra were recorded in the wavenumber range from 4000 to 400 cm^{-1} with a Perkin-Elmer Spectrum BX spectrometer using KBr pellets (3 and 300 mg, respectively).

Spectra of diffuse reflectance were recorded with a Perkin-Elmer Lambda 9 UV−vis/NIR spectrophotometer in the 200−2500 nm wavelength range in regime $F(R_d)$ Kubelka−Munk function, which can be expressed as

$$F(R_d) = \frac{(1 - R_d)^2}{2R_d}$$

where R_d is diffuse reflectance with respect to the MgO standard.

Thermal behavior of synthesized hydroxyapatites was studied gravimetrically in an experimental setup described in ref 53. A powdered sample in a Pt crucible was suspended with a Pt wire inside a vertical quartz tube in an electrical furnace with NiCr heaters. The weight of the sample was recorded continuously by an electronic balance as the sample was heated to 900 °C at the average rate of 5 °C/min, held at a constant temperature, and then cooled again to room temperature.

3. Results and Discussion

3.1. Homogeneity Regions from XRD Data. The solubility limits of rare earth elements in hydroxyapatites were determined by two methods: the "bend" (inflection) on a plot of unit cell parameters vs degree of substitution and the "disappearing phase" method.[54] In the latter case, the most intense reflection of a nonapatite phase in the experimental product was plotted against the REE content in the system's heterogeneous region. Extrapolation of this linear relationship to the intersection with the

(51) Rodriguez-Carvajal, J. *Program FullProf.2k*, version 3.40; 2005; unpublished.
(52) Roisnel, T.; Rodriguez-Carvajal, J. *Materials Sci. Forum* **2001**, *378−381*, 118−123.
(53) Prisedsky, V. V.; Vinogradov, V. M. *J. Solid State Chem.* **2004**, *177*, 4258–4268.
(54) Kachanov, N.; Mirkin, L. *Rentgenostrukturnyj analis* (*In Russian*); Moscow, Russia, 1960, p 124.

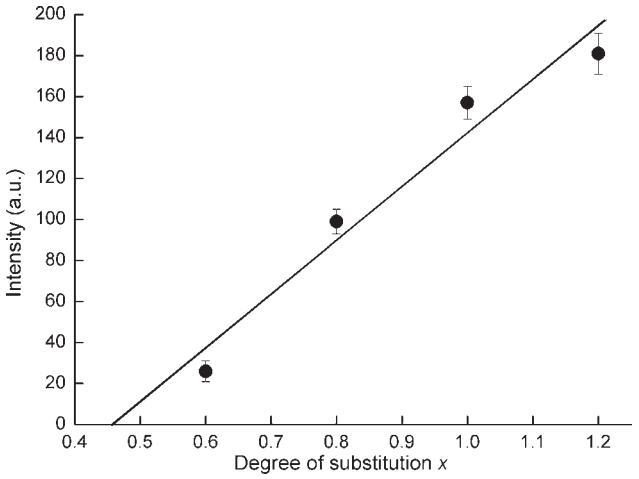

Figure 2. Plot of the intensity of (002) reflection for Tm_2O_3 vs degree of substitution, x.

abscissa axis (intensity = 0) gives an estimation for the homogeneity region boundary.

As an example, a plot of parameters a and c of the $Ca_{10-x}Tm_x(PO_4)_6(OH)_{2-x}O_x$ hexagonal unit cell vs degree of substitution by thulium (x) is shown in Figure 1. In the following, we will use thulium (Tm) as a primary example in this paper because such results on Tm substitution for calcium have not been previously published.

The substitution of Tm, which has a much smaller radius (1.134 Å), for calcium (r = 1.26 Å) causes a decrease of unit cell parameters in the homogeneity region (Figure 1). By the "bend" (inflection) in the plot of parameters a and c of the REE-substituted apatite unit cells vs degree of REE substitution, the substitution limit has been evaluated at $x = 0.45$, where x is the amount of Tm in $Ca_{10-x}Tm_x(PO_4)_6(OH)_{2-x}O_x$.

Figure 2 illustrates the refinement of the location of the single-phase region boundary using the "disappearing phase" method. We estimated the Tm substitution limit in the apatite by extrapolating the linear relationship of intensity of the largest Tm_2O_3 peak (002) vs the degree of substitution to the intersection with the abscissa axis. Accordingly, the solubility limit of Tm in $Ca_{10-x}Tm_x(PO_4)_6(OH)_{2-x}O_x$ is found at $x = 0.46$, in good agreement with the value obtained by inflection method shown in Figure 1.

The substitution limits determined for studied REE elements are presented in Table 1. The substitution limit generally decreases with increasing the REE atomic number through the series. Observed constant values of the substitution limit from La to Nd (x_{max} = 2.00) correlate with the results[55] showing a weak maximum near Nd in the uptake of REE in single-crystalline phosphate apatites.

The established variations in substitution limits with a REE atomic number are in agreement with results obtained for apatites in the vanadate system $Ca_{10-x}REE_x(VO_4)_6(OH)_{2-x}O_x$.[56,57] The narrower regions of REE solubility in vanadate apatites (x_{max} ranges from 1.30 to 0.60) relative to phosphate apatites are attributable to the lower temperatures of vanadate apatite synthesis (750−800 °C). Higher temperatures (850 °C) cause decomposition of vanadate apatite solid solutions. A similar dependence was observed also for REE-substituted strontium hydroxovanadate $Sr_{10-x}REE_x(VO_4)_6(OH)_{2-x}O_x$.[58]

3.2. IR Absorption Spectroscopy. Infrared spectra of substituted phosphate hydroxyapatite $Ca_{10-x}Tm_x(PO_4)_6(OH)_{2-x}O_x$ with x = 0, 0.2, and 0.4 are shown in Figure 3. They display bands which are identified according to ref 59. Wide intense bands in the 1090−960 and 600−460 cm^{-1} regions can be assigned to vibrations of $(PO_4)^{3-}$ ions. Additional absorption near 524 cm^{-1} in spectra of Tm-substituted apatite is due to a vibration of the Tm−O (REE−O) bond.[60] The bands in the region of 3570 and 640 cm^{-1} are due to the stretching and librational modes of the OH^- groups. Figure 3 shows that the bands of OH^- librational and stretching modes become less intense with increasing Tm substitution. The correlation of decreased OH^- content with increasing REE substitution supports an interpretation of isomorphous coupled substitution in the homogeneous region according to the scheme: $Ca^{2+} + OH^- \rightarrow REE^{3+} + O^{2-}$.

In the homogeneous region, increased Tm substitution is also correlated with decreased frequency of OH^- (ν_s) stretching modes, from 3571 to 3568 cm^{-1}, while the frequencies of librational modes (ν_l) are increased from 632 to 638 cm^{-1} (Table 2).

3.3. Diffuse-Reflectance Spectroscopy. Hydroxyapatite is optically transparent in the 200−2500 nm region of a diffuse-reflectance spectrum. However, the diffuse-reflectance spectra of Tm−hydroxyapatite solid solutions with 0.2 and 0.4 Tm atoms per 10 Ca display absorption bands characteristic of Tm^{3+} in this region. This absorption can be attributed to electron transitions between f subshells (Table 3), based on data published by White[61] and Karnall.[62]

The absorption bands are slightly different for Tm in apatite solid solutions compared to characteristic bands due to Tm^{3+} ion transitions in thulium oxide (Figure 4). The difference is shown by both displacement of the bands and changes in their relative intensities. In the Tm^{3+} spectrum, the $^3H_6 \rightarrow {}^3F_4$ transitions can be treated as hypersensitive.[63] Their intensity changes as local symmetry,[64] coordination number,[65] and degree of covalent bond REE−ligand[66] change.

Indeed, if in Tm_2O_3 spectrum the intensity of its band is rather insignificant, then in a spectrum of the solid solution it is maximal. This fact can be explained through the structure of thulium oxide, where Tm occupies two

(55) Fleet, M. E.; Liu, X; Pan, Y *J. Solid State Chem.* **2000**, *149*, 391–398.
(56) E. I. Get'man, T. A. Shul'gina, Loboda, S.N.; Marchenko, V.I.; Gromenko, M.V.; Abramenko, V.L.; Ardanova, L.I. *Ukr. Chem. J.* **2004**, *70*(8), 95−98.
(57) Get'man, E. I.; Shul'gina, T. A.; Loboda, S. N.; Carrison, L. A. *Russ. J. Inorg. Chem.* **2008**, *53*, 1342–1345.
(58) Gètman, E. I.; Yablochkova, N. V.; Loboda, S. N.; Prisedsky, V. V.; Antonovich, V. P.; Chivireva, N. A. *J. Solid State Chem.* **2008**, *181*, 2386–2392.
(59) Fowler, B. O. *Inorg. Chem.* **1974**, *13*, 194–207.
(60) Escobar, M. E.; Baran, E. J. *Monatsh. Chem.* **1982**, *113*, 43–48.
(61) White, W. B. *Appl. Spectrosc.* **1967**, *21*, 167–171.
(62) Karnall, W. T.; Fields, P. R.; Rajnak, K. *J. Chem. Phys.* **1968**, *49*, 4424–4442.
(63) *Handbook on the Physics and Chemistry of Rare Earths*, Gschneidner, K.A.; Eyring, L., Eds.; Elsevier: Amsterdam, The Netherlands, 1998, *25*, 220−224.
(64) Judd, B. R. *J. Chem. Phys.* **1966**, *44*, 839–840.
(65) Karraker., D. G. *Inorg. Chem.* **1968**, *7*, 473–479.
(66) Henrie, D. E.; Choppin, G. R. *J. Chem. Phys.* **1968**, *49*, 477–481.

Table 1. Substitution Limits x_{max} for $Ca_{10-x}REE_x(PO_4)_6(OH)_{2-x}O_x$ and $Ca_{10-x}REE_x(VO_4)_6(OH)_{2-x}O_x$

REE	La	Pr	Nd	Sm	Eu	Gd	Tb	Dy	Ho	Er	Tm	Yb
x_{max} in phosphate apatite	2.00	2.00	2.00	1.80		1.50	1.40	1.40	0.80	0.80	0.45	0.20
x_{max} in vanadate apatite	1.30		0.70	0.70	0.70	0.60						
crystal radius (r) for 8-fold coordination (Å)[48]	1.300	1.266	1.249	1.219	1.209	1.193	1.180	1.167	1.155	1.144	1.134	1.125

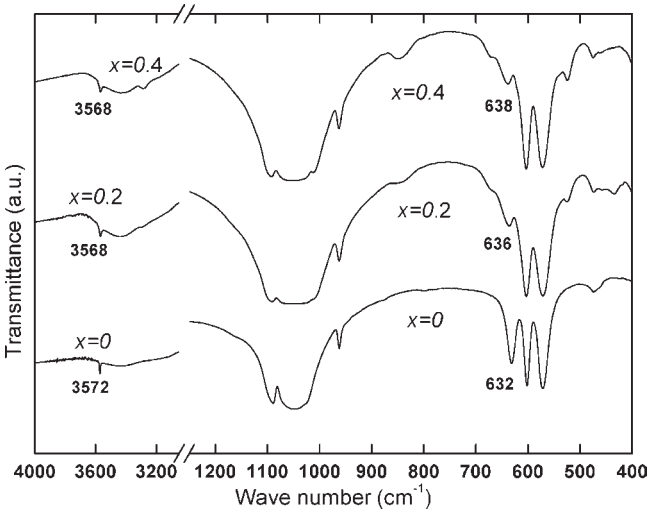

Figure 3. Infrared spectra of $Ca_{10-x}Tm_x(PO_4)_6(OH)_{2-x}O_x$ solid solutions with $x = 0$, 0.2, and 0.4.

Table 2. Distribution of Bands in IR Spectra of $Ca_{10-x}Tm_x(PO_4)_6(OH)_{2-x}O_x$

x	0	0.2	0.4
ν_s (OH)	3571	3568	3568
(H_2O)	3436	3436	3436
ν_3 (F_2) (PO_4)	1089	1091	1092
	1047	1051	1054
	(sh.)	(sh.)	1012
ν_1 (A)	962	962	962
ν_l (OH)	632	636	638
ν_4 (F_2) (PO_4)	602	603	603
	571	571	572
Tm−O		525	524
ν_2 (E) (PO_4)	474	474	474
	(sh.)	458	461
		434	

Table 3. Absorbance Maxima (nm) for Some Transitions in Solid Solution $Ca_{10-x}Tm_x(PO_4)_6(OH)_{2-x}O_x$ and Tm_2O_3 matrices

	transitions occurring from the ground-state $^3H_6$ to				
x	$^3H_4$	$^3H_5$	$^3F_4$	$^3F_3$	$^1G_4$
0.2	1610.8	1213.6	790.3	678.5	464.4
0.4	1607.6	1211.2	789.5	678.2	463.0
0.7	1606.4	1212.2	789.6	687.0	≈460
Tm_2O_3	1633.4	1206.0	795.5	683.3	462.7

crystallographically nonequivalent positions with coordination numbers 6 and local symmetry of the nearest environment D_{3d} and C_2, respectively.[67] Based on structure refinement data, Tm ions in the apatite structure preferentially occupy the low symmetry position of Ca(2) and, partially, of Ca(1) with coordination numbers 7 and 9, respectively. The frequency of vibrations due to the

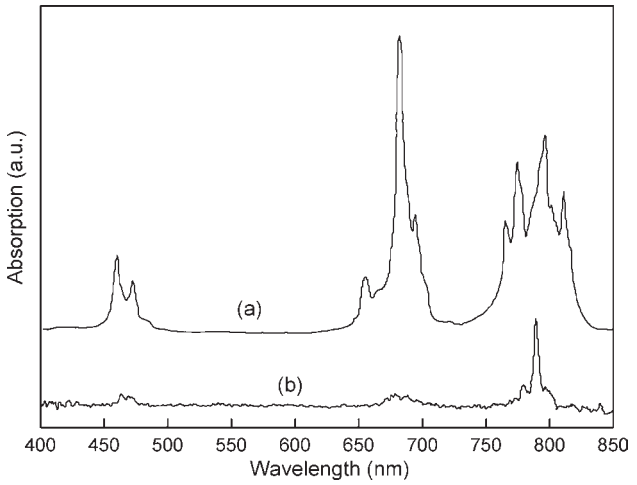

Figure 4. Diffuse-reflectance spectra of Tm_2O_3 (a) and solid solution $Ca_{9.6}Tm_{0.4}(PO_4)_6(OH)_{1.6}O_{0.4}$ (b).

$^3H_6 \rightarrow {}^3H_4$ transition decreases from 1633 to 1607 nm, with the change exceeding measurement error. The absorption at 1430 nm is found in the diffuse-reflectance spectra of studied Tm solid solutions (as well in the diffuse-reflectance spectra of Er and Ho solid solutions). The weak absorption near 1400 nm is characteristic of hydroxyapatite, unlike apatites with different composition.[68] This band can be assigned to water molecules in hydroxyapatite.

3.4. Rietveld Structure Refinement. The structural refinements were performed for calcium phosphate hydroxyapatite and its REE-substituted solid solutions $Ca_{10-x}REE_x(PO_4)_6(OH)_{2-x}O_x$. The pseudo-Voigt approximation has been used for the description of peak profiles. The final Rietveld refinement data and scanning parameters are presented for $Ca_{10-x}Tm_x(PO_4)_6(OH)_{2-x}O_x$ ($x = 0$, 0.2, and 0.4) in Table 4.

Interatomic distances calculated from the observed cell parameters and atomic coordinates are compared for substituted and unsubstituted apatites in Table 5. Atomic coordinates, isotropic thermal parameters, and crystallographic site occupancies in the apatite structure are given in Table 6 (and in Supporting Information). The crystallographic site occupancy analysis shows that Tm^{3+} ions substitute for Ca^{2+} preferentially in Ca(2) sites of the apatite structure.

Due to the location of the OH^- group at the corner of the $Ca(2)O_7$ polyhedron, the substitution $OH^- \rightarrow O^{2-}$ and $Ca^{2+} \rightarrow Tm^{3+}$ in the Ca(2) site provides local charge compensation in minimal volume and is thus favored. As shown in Table 5, as Tm substitution increases to $x = 0.4$, the Ca(2)−O(OH) and Ca(2)−Ca(2) distances decrease by 0.060 and 0.092 Å, respectively. However, the mean distance Ca(2)−O(1−3) does not change noticeably in

(67) Gubanov, V.A.; Kurmayev, E.Z.; Ivanovsky, A.L. *Quantum chemistry of solid phase* (*in Russian*); The Science: Moscow, Russia, 1984.

(68) Lane, M.D.; Dyar, M.D.; Bishop, J.L. *Lunar and Planetary Science XXXVIII*; Lunar and Planetary Institute: Houston, TX, 2007.

spite of the ionic radius of Tm^{3+} being smaller than that of Ca^{2+}. Earlier works[49,50] showed that a substitution of La^{3+} ion, which is slightly larger than Ca^{2+}, and Dy^{3+} ion, which is slightly smaller than Ca^{2+}, both produce an elongation of Ca(2)−O(1−3) distances in the coordination polyhedron. In the case of Dy^{3+}, an increase of the mean distance between Ca(2) and its six coordinating oxygen atoms is caused by repulsion between O(1−3) and OH^- (O^{2-}) ions which approach Ca(2)Dy^{3+} in the channels of apatite structure. This shift of the OH^-(O^{2-}) ions results from strong electrostatic interaction due to replacement of Ca^{2+} and OH^- ions by more highly charged Dy^{3+} and O^{2-} ions. The substitution of O^{2-} for OH^- in the channels of the Tm−apatite structure causes a decrease in both Ca(2)−O(OH) and Ca(2)−Ca(2) distances, whereas other Ca(2)−O(1−3) mean distances in the seven-fold coordination polyhedron do not change noticeably. As in the case of the Dy^{3+}-substituted apatites, the anticipated decrease of Ca(2)−O(1,2,3) interatomic distances due to the smaller radius of Tm^{3+} is more than offset by electrostatic repulsion between O^{2-} ions in the $Ca(2)O_7$ coordination polyhedron and OH^- or O^{2-} ions in nearby structural channels.

Table 4. Rietveld Refinement for $Ca_{10-x}Tm_x(PO_4)_6(OH)_{2-x}O_x$

degree of Tm substitution x (per 10 Ca)	0	0.2	0.4
space group		$P6_3/m$	
structure type		apatite	
cell parameters			
a, Å	9.4190(2)	9.4088(2)	9.4056(2)
c, Å	6.8812(2)	6.8712(2)	6.8641(2)
cell volume, Å^3	528.69(2)	526.78(2)	525.88(2)
radiation, wavelengths $\lambda\alpha_1$ and $\lambda\alpha_2$, Å	Cu K_α	1.54056	1.54439
number of measured reflections	776	772	772
number of refinement parameters	37	36	36
reliability factors			
R_B	7.70	8.41	7.99
R_F	5.75	6.15	5.34
R_P	11.0	6.77	5.89
R_{WP}	14.6	8.67	7.76
χ^2	1.36	2.01	1.91

Table 5. Selected Interatomic Distances $Ca_{10-x}Tm_x(PO_4)_6(OH)_{2-x}O_x$ for Varying Values of x

	x = 0	x = 0.2	x = 0.4
Ca(1)−O(1) × 3	2.358(8)	2.367(7)	2.362(8)
Ca(1)−O(2) × 3	2.460(8)	2.473(7)	2.468(8)
Ca(1)−O(3) × 3	2.772(8)	2.793(7)	2.767(8)
<Ca(1)−O>	2.530	2.544	2.532
Ca(2)−O(1)	2.691(10)	2.708(8)	2.737(9)
Ca(2)−O(2)	2.365(12)	2.369(10)	2.367(11)
Ca(2)−O(3) × 2	2.559(7)	2.542(6)	2.542(6)
Ca(2)−O(3) × 2	2.292(6)	2.295(5)	2.310(6)
<Ca(2)−O(1−3)>	2.460	2.459	2.468
Ca(2)−O(4)	2.404(5)	2.371(4)	2.344(4)
<Ca(2)−O>	2.452	2.446	2.450
P−O(1)	1.592(12)	1.569(10)	1.572(10)
P−O(2)	1.530(12)	1.528(10)	1.533(11)
P−O(3) × 2	1.577(6)	1.575(6)	1.567(6)
<P−O>	1.569	1.562	1.560
Ca(2)−Ca(2)	4.084(6)	4.024(5)	3.992(5)
O(3)−O(4)	3.055(9)	3.027(8)	3.063(7)

To investigate primary controls on interionic distances in the apatite structure, we present a summary of structural analysis data for earlier studied systems and $Ca_{10-x}Tm_x(PO_4)_6(OH)_{2-x}O_x$ in Table 6. REE substitution limits (Table 1) in hydroxyapatite decrease with increasing atomic number in the La−Yb series. A lanthanide contraction occurring in the elements starting at La can explain a monotonic increasing difference in ionic radii between Ca and REE: from 0.006 Å for r(Ca) − r(Pr) to 0.135 Å for r(Ca) − r(Yb) . Therefore, decrease of substitution limits of REE for Ca correlates with the increasing difference in radii between Ca and the substituting REE, r(Ca) − r(REE), in the series. And this is in apparent agreement with a control of substitution by spatial accommodation of REE substituents as the difference in radii between calcium and REE, r(Ca) − r(REE), increases in the same direction. REE occupancy in the Ca(2) site and the [REE−Ca(2)]/ [REE−Ca(1)] ratio also decreased with increasing REE atomic number, but it is not clear from our data whether this behavior depends on the nature of the REE in the apatite structure or on the number of REE atoms in the apatite formula (value of x is decreased from 2.0 to 0.4). As a result of substitution of REE with increasing atomic number (decreasing ionic radius), the mean Ca(2)−O(OH) and Ca(2)−Ca(2) distances decrease as expected (Table 6), whereas the mean Ca(2)−O(1−3) distances increase not only for the larger La^{3+} ion but also for the smaller rare earth ions as well. This observation shows that interionic distances depend not only on radii of the ions involved in the substitution but on their charges as well. The shift of six O^{2-} ions away from Ca^{2+}(2) in the coordination polyhedron brings them closer to P^{5+} ions and results in a decrease of the mean P−O distances. This unexpected observation demonstrates that in the given model of substitution, the variation of the

Table 6. Site Occupancies and Interatomic Distances for REE-Substituted $Ca_{10-x}REE_x(PO_4)_6(OH)_{2-x}O_x$

REE	La[49]	Nd[50]	Sm	Gd	Dy[50]	Tm	unsubstituted Ca hydroxyapatite
degree of substitution, x	2.0	2.0	1.6	1.4	1.4	0.4	0.0
occupancy Ca(1)							
Ca	1.000	0.983	0.971	0.975	0.967	0.992	1.000
REE		0.017	0.029	0.025	0.033	0.009	
occupancy Ca(2)							
Ca	0.666	0.678	0.753	0.783	0.789	0.939	1.000
REE	0.333	0.322	0.248	0.217	0.211	0.061	
[REE−Ca(2)]/[REE−Ca(1)]		18.9	8.6	8.7	6.4	6.8	1.0
distance Ca(2)−O(1−3), Å	2.560	2.542	2.527	2.494	2.510	2.469	2.460
distance Ca(2)−Ca(2), Å	3.711	3.747	3.811	3.827	3.840	3.992	4.052
distance Ca(2)−(OH)O(4), Å	2.143	2.175	2.220	2.241	2.218	2.344	2.380
distance P−O, Å	1.541	1.540	1.542	1.552	1.530	1.560	1.563
crystal radius r, Å	1.300	1.249	1.219	1.193	1.167	1.134	1.26
r(Ca) − r(REE), Å	−0.040	0.011	0.041	0.067	0.093	0.126	
[r(Ca) − r(REE)]/r(Ca), %	−3.1	0.9	3.3	5.3	7.4	10.0	

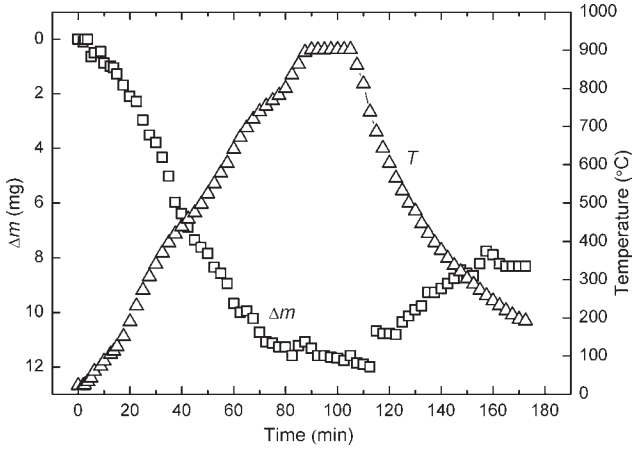

Figure 5. Weight change for a sample of hydroxyapatite subjected to a heating−cooling cycle.

interionic distances is controlled mainly by charges of the ions involved in the substitution and to a lesser extent by their sizes.

The established variations in substitution limits and interatomic distances with REE atomic number are in agreement with results obtained for apatites in the system $Ca_{10-x}REE_x(VO_4)_6(OH)_{2-x}O_x$.[56,57] The narrower regions of REE solubility in vanadate apatites (x_{max} ranges from 0.12 to 1.30 for systems $Ca_{10-x}Y_x(VO_4)_6(OH)_{2-x}O_x$ and $Ca_{10-x}La_x(VO_4)_6(OH)_{2-x}O_x$, respectively) relative to phosphate apatites are attributable to the lower temperatures of vanadate apatite synthesis (750−800 °C). Higher temperatures (850 °C) cause decomposition of vanadate apatite solid solutions.

3.5. Thermal Behavior of Hydroxyapatite. The ability of hydroxyapatites to adsorb molecules on their surfaces is important in their application as catalysts, sorbents, and wet sensors. To examine this ability of hydroxyapatite, samples have been studied gravimetrically in the temperature range 20−900 °C.

Weight loss of the sample upon heating (example in Figure 5) has a nonmonotonic character, likely due to desorption of surface-bound water. Upon cooling, water is reversibly absorbed starting at about 500 °C. Plots of such samples show a characteristic indistinct transition between the regions of poorly and strongly bonded water.[1] Figure 5 shows such a transition at an inflection point at approximately 130 °C. On heating to 900 °C, weight loss of the 0.7230 g sample was 11.76 mg, corresponding to a mass fraction of water of 1.63%. Hence, at room temperature, a composition of $Ca_{10}(PO_4)_6(OH)_2 \cdot 0.9H_2O$ can be assigned to hydroxyapatite. Based on a similar investigation, hydroxovanadate can be described by the composition $Ca_{10}(VO_4)_6(OH)_2 \cdot H_2O$. REE substitutions do not affect thermal behavior of hydroxyapatite absorption and removal of water in heating−cooling cycles.

4. Conclusions

Trivalent rare earth ions substitute for calcium preferentially at Ca(2) sites in hydroxyapatites $Ca_{10-x}REE_x(PO_4)_6(OH)_{2-x}O_x$. Due to the increasing difference in radii between Ca and rare earth elements (REE) in the series caused by lanthanide contraction, substitution limits of REE for Ca in a series from La^{3+} to Yb^{3+} decrease from $x_{max} = 2.00$ to 0.20. A similar tendency for substitution limits was found for vanadate apatite. As a result of substitution, the mean Ca(2)−O(OH) and Ca(2)−Ca(2) distances decrease, whereas the mean distances Ca(2)−O(1−3) increase not only for the larger La^{3+} ions but also for smaller rare earth ions as well. This unexpected fact demonstrates that the changes in interatomic distances are controlled not only by the geometrical factor, the difference in sizes of the ions involved in the substitution, but also by their charges as well. This finding has practical importance for choosing new substituents and enhancing adsorptive, catalytic, and other important properties of hydroxyapatite.

Acknowledgment. The authors would like to acknowledge Minnesota State University, Mankato, Minnesota, U.S.A. for the faculty research grant supporting this investigation. The authors are grateful to Dr. Steven Losh for editorial help.

Supporting Information Available: Crystallographic information files (CIF) of $Ca_{10-x}Tm_x(PO_4)_6(OH)_{2-x}O_x$ ($x = 0$, 0.2, and 0.3).This material is available free of charge via the Internet at http://pubs.acs.org.